Workflow for Fast Lipid Tissue Screening using LESA-FT-ICR-MS

Jean R. N. Haler,[a] Emma K. Sisley,[b,c] Yarixa L. Cintron-Diaz,[a] Sanjib N. Meitei,[d] Helen J. Cooper,[b] Francisco Fernandez-Lima*[a,e]

Lipid screening of biological substrates is an important component during biomarker detection and identification. In this work, a fast workflow is described capable of rapid screening for lipid components from biological tissues at ambient pressure based on liquid microjunction extraction in tandem with nano-electrospray ionization (nESI) with ultra-high resolution mass spectrometry, i.e., liquid extraction surface analysis (LESA) coupled to Fourier-transform ion cyclotron resonance (tandem) mass spectrometry (LESA-FT-ICR-MS/MS). Lipid profiles are presented for thin tissue sections of mouse brain (MB) and liver (ML) sample, analyzed in both positive and negative mode by data-dependent acquisition (DDA) tandem FT-ICR-MS/MS. Candidate assignments were based on fragmentation patterns using mostly SimLipid software and accurate mass using mostly the LipidMaps database (average sub-ppm mass error). A typical, single point surface analysis (< 1 mm spatial sampling resolution) lasted less than 15 minutes and resulted in the assignment of (unique and mulitple) lipid identifications of ~190 (MB) and ~590 (ML) *m/z* values. Despite the biological complexity, this led to unique identifications of distinct lipid molecules (sub-ppm mass error) from 38 different lipid classes, corresponding to 10-30% of the lipid *m/z* identifications.

Introduction

Lipids are important components of living cells and frequently mediate biological processes.[1] Changes to a cell's environment are rapidly translated into changes in its lipid composition, making it an attractive target for biomarker discovery and disease screening and treatment.[1–3] Lipid analyses are typically performed using mass spectrometry (MS).[1,3–8]

Lipid MS analyses can be undertaken at several levels. For example, the sum composition of the fatty acids constituting a lipid can obtained with an exact mass MS measurement (e.g. PC(40:6)); moreover, tandem MS (MS/MS) experiments, such as collision induced dissociation (CID), can further allow to elucidate the length and the number of double bonds of each of the fatty acid chains (e.g. PC(20:2_20:4)). The double bond positions on the fatty acid chains can also be investigated through specific fragmentation techniques.[9–14] The coupling of different separation techniques in front of the MS analysis, such as liquid chromatography (LC) or ion mobility (IM), can add an additional separation dimension to the MS lipid characterization.[5,15–19]

The challenges for global mass spectrometry analyses of lipids (lipidomics) are twofold. First, the sample preparation can bias the lipid composition by selecting only a partial lipid content of the sample.[4,5] Second, the mass spectrometry analysis must be capable of detecting both low and high abundance species, with a high resolving power and mass

accuracy in order to resolve and confidently identify isobaric lipids. The latter challenge can be addressed by using instruments such as Fourier-transform ion cyclotron resonance mass spectrometers (FT-ICR MS). The choice of the sample preparation however depends on the ionization method used for the mass spectrometry analysis. For tissue analyses, imaging techniques such as secondary ion mass spectrometry (SIMS) or matrix assisted laser desorption ionization (MALDI) mass spectrometry are often used.[20–28] Ionization suppression and the matrix choice potentially bias the observed lipid composition.[5,21,28,29] When using electrospray ionization (ESI), the MS analyses are usually preceded by LC separations with long separation gradients (up to 2 hours) depending on the LC column, the LC solvent conditions, and the numbers of lipid classes.[30] LC-LC couplings have shown some advantages in lipid separations, with the tradeoff of increased analysis times.[5,15]

An alternative to lipid extraction (e.g., LC-MS/MS) or surface mapping (i.e., desorption electrospray ionization (DESI)[31–34] or MALDI), is liquid extraction surface analysis (LESA) in which a liquid microjunction between the surface and an extraction tip is created, followed by direct nano-electrospray infusion.[35–37] In a LESA experiment, the solvent (or solvent mixtures) of choice can direct the type of chemical class that is extracted (e.g.,. lipids or proteins).[38–48] The choice of solvent composition in LESA can favor the extraction of certain lipid classes.[46–49] When compared to an LC-MS/MS or a MALDI-MS/MS experiment, LESA-MS/MS significantly decreases the sample preparation time and potential ionization suppression bias (e.g., MALDI matrix). Moreover, LESA experiments lead to continuous sample infusions during several minutes, which allows performing MS/MS measurements for lipid identification, with the potential of adding spatial tissue profiling to the analyses.[41]

Here, we developed a fast, screening lipid workflow based on LESA-FT-ICR-MS and MS/MS for ambient analysis of thin tissue sections. Examples shown include mouse brain and mouse liver analyzed using data dependent acquisition (DDA) with ultra-high mass resolution and high mass accuracy in positive and negative ion mode. Candidate lipid assignments were performed using different databases, based on MS/MS fragmentation patterns, as well as on MS1 accurate mass measurements (< 3 ppm mass accuracy database searches).

Experimental

Thin Tissue Sections

Liver and brain from wildtype mice (extraneous tissue from culled animals) were the gift of Prof. Steve Watson (University of Birmingham). Organs were frozen on dry ice prior to storage at -80 °C. Sections of murine liver tissue and brain tissue of area ~1.5 cm^2 were obtained at a thickness of 10 μm using a CM1850 Cryostat (Leica Microsystems, Wetzlar, Germany) and thaw mounted onto glass slides.

LESA-MS/MS analysis

Thin tissue section samples were loaded onto a universal LESA adapter plate and placed in the TriVersa Nanomate chip-based electrospray device (Advion, Ithaca, NY) coupled to a 7T Solarix XR FT-ICR MS (Bruker Daltonics, Germany). The solvent was EtOH/H_2O/HCOOH 80/19.9/0.1 (v/v/v). It allowed to extract similar lipid classes than with other solvent mixtures.[46–49] A total of 6 µL were aspirated from the solvent well. The robotic arm relocated to a position above the tissue and descended to a height 0.2 mm above the surface of the sample. A total of 3 µL of the solution was dispensed onto the sample surface to form a liquid microjunction. The liquid microjunction was maintained for 5 seconds; then 3.5 µL were reaspirated into the pipet tip. This liquid dispensing and reaspiration was repeated twice before MS injection.

The FT-ICR MS instrument was operated in both negative and positive ionization mode and data were collected for 15 minutes. Data dependent acquisition of MS/MS spectra was performed using the AutoMS/MS function and spectra were recorded with 500kW. CID was utilized as a fragmentation tool (typically 15-35 eV), with nominal mass quadrupole isolation prior to injection into the CID cell. Spectra were externally calibrated using a Tuning Mix solution (Agilent, SC)[50] and internally calibrated using single point correction with identified lipids. For example, the internal recalibration was performed using PC(34:1) (*m/z = 760.5851*) for MB and using PC(34:2) (*m/z = 758.5694*) for ML in positive mode and PC(34:1) (*m/z = 804.5760*) for MB and using PC(34:2) (*m/z = 802.5604*) for ML in negative mode. Data was analyzed using DataAnalysis 5.2 (Bruker Daltonics, Germany) and SimLipid software (Premier Biosoft, US). Assignments were manually curated using Alex123[51] and the LIPID MAPS Lipidomics Gateway[52,53]. MS1 exact mass identifications were performed using the LIPID MAPS Lipidomics Gateway[52,53] with a ± 3 ppm mass error search criterion. During lipid candidate assignments, protonated species (with and without the loss of H_2O according to the lipid class), sodium and potassium cation adduct species were considered for positive mode; deprotonated species, chloride and formate anion adduct species were considered for negative mode analysis. Lipids with odd sum compositions were discarded as biologically unlikely when multiple identification possibilities were found, but the assignments were kept if they constituted unique identifications within the ± 3 ppm mass error search. MS1 exact mass measurements were recorded with 4MW and 2MW for positive and negative modes, respectively. The mass resolution was around 170,000 at *m/z* 760.5851 and 758.5694 for positive mode MB and ML, respectively and around 60,000 at *m/z* 804.5760 and 802.5604 for negative mode MB and ML, respectively. For data completeness, targeted MS/MS after preliminary MS1 lipid assignment was performed on species where only little interfering *m/z* peaks were found in the spectra, using an Impact Q-ToF instrument (Bruker Daltonics Inc., Billerica, MA).

Results and Discussion

The fast lipid screening workflow is based on LESA of thin tissue sections (without any other surface treatment) followed by ultra-high-resolution MS/MS analysis (see Figure 1). The full-scan MS1 analyses and DDA MS/MS take advantage of the ultra-high mass resolution and high mass accuracy of the FT-ICR mass spectrometers. For example, during DDA using CID as a fragmentation method, typical neutral losses and lipid headgroups were utilized during candidate assignment with high mass accuracy. While not the focus of this paper, it should be noted that other MS/MS fragmentation techniques (e.g., EID, OzID, CTD)[9–14] may be easily implemented and provide better and/or complementary structural information during lipid candidate assignment. In the proposed workflow, an initial search provides candidate lipids from the DDA dataset. Following DDA interpretation, the MS1 spectrum is processed (i.e., internal single point correction) and a list of monoisotopic *m/z* signals is created. This list is used to search among lipid databases using mass accuracy as a criterion. In many cases, the accurate mass database search will return multiple lipid hits, which will require secondary analysis (e.g., targeted MS/MS experiments). While not currently implemented, online processing of the MS1 scan using accurate mass lipid database searches can be performed to retrofit the DDA acquisition target list; this procedure can be easily implemented during static nESI since no major changes in the spray occur during 15 minutes, and each MS/MS acquisition requires typically 10-20 seconds.

The LESA-FT-ICR-MS (MS1 and MS/MS) analysis of two biological substrates (i.e., mouse brain, MB, and mouse liver, ML) resulted in the unique identification (within a ± 3 ppm database search for MS1) of distinct lipids from 38 different lipid classes in the 400-1000 *m/z* range. The unsupervised analysis resulted in the identification of ~190 (MB) and ~590 (ML) monoisotopic *m/z* peaks as lipids. Despite the biological complexity, 10-30% of these lipid identifications yielded unique lipid assignments (in contrast to multiple lipid assignments to one *m/z* peak; see Figure 2). The comparison of the MB and ML MS1 profiles (either positive or negative ionization mode) shows abundant lipid signal in the 700-900 *m/z* range. Overall, a larger number of monoisotopic *m/z* peaks were observed and picked in the ML sample when compared to the MB sample (e.g., 226(MS+)/2215(MS-) for ML and 157(MS+)/174(MS-) for MB (see supplementary information Figure SI1 for an extract of the negative mode spectra)). Figure 3 highlights the importance of performing these analyses using ultra-high-resolution mass spectrometers such as FT-ICR. Between *m/*z 738.2 and 738.8, 5 out of the 6 *m/z* values were correlated to lipid identifications.
In positive mode, the most intense *m/*z peaks with unique lipid identifications correspond to phosphatidylcholines (PC) in the MB and ML samples, with minor lipid signals corresponding to PE, LPC, DG, MGDG, SM, PS, CAR, Cer, HexCer, LPS, LacCer, LPIP, MG, PI-Cer, S1P, DGDG, LPA, MIPC and PG (see Table 1 and Figure 4.a. and c.; all abbreviations are described in the supplementary information). For the case of PC, the AutoMS/MS identification (without fatty acid chain or double bond identification) relied mostly on the detection of the headgroup and the neutral loss of a fatty acid chain; other

lipids assignments were mostly based on MS1 accurate mass. Tables SI1 and SI2 in the supplementary information summarize all MS1 *m/z* signals with multiple lipid identifications within the ± 3 ppm database search. It should be noted that multiple adducts were observed for the most abundant lipids, increasing the confidence during their identifications. All uniquely-identified lipids yielded sub-ppm average *m/z* deviation (e.g., 0.70 ppm for MB and of -0.85 ppm for ML).

In negative mode, the lipid classes with the most unique identifications correspond to phosphatidylethanolamines (PE), LPE, PC and SHexCer in MB, and to phosphatidylserines (PS), fatty acyls (FA), glycerophosphoglycerols (PG) and LPS in ML (see Figure 4.b and d., Tables SI3 and SI4). Most of the AutoMS/MS assignments were based on the observation of the fatty acid losses and fragments; other lipids assignments were mostly based on MS1 accurate mass (see supplementary tables SI3 and SI4). Tables SI5 and SI6 in the supplementary information summarize all MS1 *m/z* signals with multiple lipid identifications within the ± 3 ppm database search. For example, 64 out of the 174 picked *m/z* values for MB and 437 out of the 2215 values for ML were identified with unique or multiple matches. Further dataset descriptions can be found in Figure SI2 for both MB and ML in positive and negative ionization. All uniquely-identified lipids yielded sub-ppm average *m/z* deviation (e.g., 0.27 ppm for MB and 0.02 ppm for ML).

An estimate of the specificity of the LESA-FT-ICR-MS workflow as a function of the biological surface was obtained from the comparison of the unique lipid assignments in the MB and ML (see Figure 5, including both positive and negative mode MS1 and MS/MS identifications). 25 lipids were found common to the MB and ML, with the most abundant being 8 PC, 3PE, 3 LPE, and 3 LPC. One lipid from the LPI, LPS, MG, S1P, SHexCer, SM, SQDG, and TG classes were found to be common. In the case of MB, 20 different lipid classes were identified (ranked according to the number of identified lipids: PC, PE, LPS, LPE, LPC, SHexCer, PS, SQDG, LacCer, SM, PG, Cer, DG, TG, LPI, CerP, PI-Cer, MG, CAR, and S1P. The most abundant lipid class for MB was PC (16 lipids), followed by PE (15 lipids) (see Table SI7). In the case of ML, 38 different lipid classes were identified (ranked according to the number of identified lipids: PS, FA, PC, PE, PG, LPS, LPE, Cer, DG, TG, MGDG, LPC, LPA, SQDG, LPI, LPG, PA, MG, PI, LacCer, SM, CerP, PI-Cer, HexCer, LacSph, LPIP, NAE; SHexSph, CAR, MIPC, PIP, WE, SHexCer, S1P, DGDG, HexSph, NAT, and PE-Cer). The most abundant lipid class for ML was PS (28 lipids), followed by FA and PC (19 lipids each), and PE (16 lipids) (see Table SI5).

An example of the use of targeted MS/MS following the MS1 accurate mass search is shown for the case of MB in negative ion mode (see Table 2). The added fragment ion information enables the exclusion of accurate mass identifications as well as to increase the structural information. For example, the identification of PE(22:6_16:0) (*m/z = 762.5079*) and PE(20:4_18:0) (*m/z = 766.5393*) is illustrated in Table 2.

Conclusions.

A fast and high-throughput analysis workflow for lipid screening in biological tissues at ambient conditions without the need for pre-separations or sample treatment is shown. The LESA-FT-ICR MS(/MS) analysis of mouse brain and liver sections resulted in the identification of 38 lipid classes in a single analysis (< 15 min), with lipid markers specific to each tissue. The combination of accurate mass and AutoMS/MS resulted in the identification of unique and common lipid molecules from the biological tissues, with average sub-ppm mass accuracy. The workflow was presented using CID as a proof of concept, but other fragmentation techniques providing further structural lipid information are equally suitable. The most abundant lipids species are typically observed and identified in several adduct forms (e.g., protonated, sodiated and potassiated), thus increasing the confidence in the molecular assignment. In the examples shown, ~190 (MB) and ~590 (ML) *m/z* values were identified by unique or multiple lipid assignments in positive and negative mode, with 10-30% of these identifications being unique and distinct lipids assignments. In addition to MS analysis, further integration on post-ionization mobility separation can provide additional structural information. [15–19]

Conflicts of interest

There are no conflicts to declare.

Acknowledgements

The work at FIU was supported by a National Institute of Allergy and Infectious Diseases (R21AI135469) and a NSF CAREER (CHE-1654274), with co-funding from the Division of Molecular and Cellular Biosciences to FFL. JRNH acknowledges the Fulbright for financial support. The work at UoB was supported by a IAS Vanguard Fellowship to FFL. HJC is an EPSRC Established Career Fellow (EP/L023490/1). EKS is funded by the EPSRC via the Centre for Doctoral Training in Physical Sciences for Health (Sci-Phy-4-Health) (EP/L016346/1), in collaboration with UCB Pharma. The FT-ICR mass spectrometer used in this work was funded by BBSRC (BB/M012492/1). Supplementary data supporting this research is openly available from the University of Birmingham data archive.

References

1 A. Shamim, T. Mahmood, F. Ahsan, A. Kumar and P. Bagga, *Clin. Nutr. Exp.*, 2018, **20**, 1–19.

2 E. R. Schenk, F. Nau, C. J. Thompson, Y. C. Tse-Dinh and F. Fernandez-Lima, *J. Mass Spectrom.*, 2015, **50**, 88–94.

3 K. Yang and X. Han, *Trends Biochem. Sci.*, 2016, **41**, 954–969.

4 G. Dawson, *Biochim. Biophys. Acta - Mol. Cell Biol. Lipids*, 2015, **1851**, 1026–1039.
5 C. Giles, R. Takechi, V. Lam, S. S. Dhaliwal and J. C. L. Mamo, *Prog. Lipid Res.*, 2018, **71**, 86–100.
6 P. H. Axelsen and R. C. Murphy, *J. Lipid Res.*, 2010, **51**, 660–671.
7 H. C. Lee and T. Yokomizo, *Biochem. Biophys. Res. Commun.*, 2018, **504**, 576–581.
8 Y. H. Rustam and G. E. Reid, *Anal. Chem.*, 2018, **90**, 374–397.
9 X. Zheng, R. D. Smith and E. S. Baker, *Curr. Opin. Chem. Biol.*, 2018, **42**, 111–118.
10 H. J. Yoo and K. Håkansson, *Anal. Chem.*, 2010, **82**, 6940–6946.
11 J. W. Jones, C. J. Thompson, C. L. Carter and M. A. Kane, *J. Mass Spectrom.*, 2015, **50**, 1327–1339.
12 S. R. Ellis, H. T. Pham, M. In het Panhuis, A. J. Trevitt, T. W. Mitchell and S. J. Blanksby, *J. Am. Soc. Mass Spectrom.*, 2017, **28**, 1345–1358.
13 P. Li and G. P. Jackson, *J. Mass Spectrom.*, 2017, **52**, 271–282.
14 M. C. Thomas, T. W. Mitchell, D. G. Harman, J. M. Deeley, J. R. Nealon and S. J. Blanksby, *Anal. Chem.*, 2008, **80**, 303–311.
15 A. Baglai, A. F. G. Gargano, J. Jordens, Y. Mengerink, M. Honing, S. van der Wal and P. J. Schoenmakers, *J. Chromatogr. A*, 2017, **1530**, 90–103.
16 W. B. Ridenour, M. Kliman, J. A. McLean and R. M. Caprioli, *Anal. Chem.*, 2010, **82**, 1881–1889.
17 J. C. May, C. R. Goodwin and J. A. McLean, *Curr. Opin. Biotechnol.*, 2015, **31**, 117–121.
18 J. C. May, C. R. Goodwin, N. M. Lareau, K. L. Leaptrot, C. B. Morris, R. T. Kurulugama, A. Mordehai, C. Klein, W. Barry, E. Darland, G. Overney, K. Imatani, G. C. Stafford, J. C. Fjeldsted and J. A. McLean, *Anal. Chem.*, 2014, **86**, 2107–2116.
19 C. Hinz, S. Liggi and J. L. Griffin, *Curr. Opin. Chem. Biol.*, 2018, **42**, 42–50.
20 B. M. Prentice, J. C. McMillen and R. M. Caprioli, *Int. J. Mass Spectrom.*, , DOI:10.1016/j.ijms.2018.06.006.
21 B. M. Ham, J. T. Jacob and R. B. Cole, *Anal. Chem.*, 2005, **77**, 4439–4447.
22 A. P. Bowman, R. M. A. Heeren and S. R. Ellis, *TrAC - Trends Anal. Chem.*, 2018, 1–10.
23 F. Barré, B. Rocha, M. Towers, P. Murray, E. Claude, B. C. Pastor, R. Heeren and T. P. Siegel, *Int. J. Mass Spectrom.*, , DOI:10.1016/j.ijms.2018.09.015.
24 M. L. Kraft and H. A. Klitzing, *Biochim. Biophys. Acta - Mol. Cell Biol. Lipids*, 2014, **1841**, 1108–1119.
25 K. J. Adams, J. D. DeBord and F. Fernandez-Lima, *J. Vac. Sci. Technol. B, Nanotechnol. Microelectron. Mater. Process. Meas. Phenom. JVST B*, 2016, **34**, 51804.
26 P. Sjövall, B. Johansson and J. Lausmaa, *Appl. Surf. Sci.*, 2006, **252**, 6966–6974.
27 H. Tian, J. S. Fletcher, R. Thuret, A. Henderson, N. Papalopulu, J. C. Vickerman and N. P. Lockyer, *J. Lipid Res.*, 2014, **55**, 1970–1980.
28 D. Gode and D. A. Volmer, *Analyst*, 2013, **138**, 1289–1315.
29 S. R. Ellis, S. H. Brown, M. In Het Panhuis, S. J. Blanksby and T. W. Mitchell, *Prog. Lipid Res.*, 2013, **52**, 329–353.

30 Y. Satomi, M. Hirayama and H. Kobayashi, *J. Chromatogr. B Anal. Technol. Biomed. Life Sci.*, 2017, **1063**, 93–100.
31 A. L. Rennó, M. Alves-Júnior, N. V. Schwab, M. N. Eberlin, A. A. Schenka and A. Sussulini, *Int. J. Mass Spectrom.*, 2017, **418**, 86–91.
32 J. I. Zhang, N. Talaty, A. B. Costa, Y. Xia, W. A. Tao, R. Bell, J. H. Callahan and R. G. Cooks, *Int. J. Mass Spectrom.*, 2011, **301**, 37–44.
33 M. Manikandan, Z. Kazibwe, N. Hasan, A. Deenadayalan, J. Gopal, T. Pradeep and S. Chun, *TrAC Trends Anal. Chem.*, 2016, **78**, 109–119.
34 L. S. Eberlin, C. R. Ferreira, A. L. Dill, D. R. Ifa and R. G. Cooks, *Biochim. Biophys. Acta - Mol. Cell Biol. Lipids*, 2011, **1811**, 946–960.
35 V. Kertesz, M. J. Ford and G. J. Van Berkel, *Anal. Chem.*, 2005, **77**, 7183–7189.
36 T. Wachs and J. Henion, *Anal. Chem.*, 2001, **73**, 632–638.
37 V. Kertesz and G. J. Van Berkel, *J. Mass Spectrom.*, 2010, **45**, 252–260.
38 R. L. Griffiths and H. J. Cooper, *Anal. Chem.*, 2016, **88**, 606–609.
39 N. J. Martin, R. L. Griffiths, R. L. Edwards and H. J. Cooper, *J. Am. Soc. Mass Spectrom.*, 2015, **26**, 1320–1327.
40 S. A. Murfitt, P. Zaccone, X. Wang, A. Acharjee, Y. Sawyer, A. Koulman, L. D. Roberts, A. Cooke and J. L. Griffin, *J. Proteome Res.*, 2018, **17**, 946–960.
41 E. C. Randall, A. M. Race, H. J. Cooper and J. Bunch, *Anal. Chem.*, 2016, **88**, 8433–8440.
42 M. Wisztorski, A. Desmons, J. Quanico, B. Fatou, J. P. Gimeno, J. Franck, M. Salzet and I. Fournier, *Proteomics*, 2016, **16**, 1622–1632.
43 R. L. Griffiths, A. J. Creese, A. M. Race, J. Bunch and H. J. Cooper, *Anal. Chem.*, 2016, **88**, 6758–6766.
44 R. L. Griffiths, K. I. Kocurek and H. J. Cooper, *Curr. Opin. Chem. Biol.*, 2018, **42**, 67–75.
45 V. A. Mikhailov, R. L. Griffiths and H. J. Cooper, *Int. J. Mass Spectrom.*, 2017, **420**, 43–50.
46 Z. Hall, Y. Chu and J. L. Griffin, *Anal. Chem.*, 2017, **89**, 5161–5170.
47 N. N. Zhao, Y. F. Sun, L. Zong, S. Liu, F. R. Song, Z. Q. Liu and S. Y. Liu, *Int. J. Mass Spectrom.*, 2018, **434**, 29–36.
48 L. Zong, Z. Pi, S. Liu, J. Xing, Z. Liu and F. Song, *Rapid Commun. Mass Spectrom.*, 2018, **32**, 1683–1692.
49 R. Nitsch, J. Baumgart, J. Vogt, C. S. Ejsing, R. Almeida, Z. Berzina and E. C. Arnspang, *Anal. Chem.*, 2014, 87, 1749–1756.
50 1999, 19.
51 J. K. Pauling, M. Hermansson, J. Hartler, K. Christiansen, S. F. Gallego, B. Peng, R. Ahrends and C. S. Ejsing, *PLoS One*, 2017, **12**, 1–21.
52 E. Fahy, S. Subramaniam, H. A. Brown, C. K. Glass, A. H. Merrill, R. C. Murphy, C. R. H. Raetz, D. W. Russell, Y. Seyama, W. Shaw, T. Shimizu, F. Spener, G. van Meer, M. S. VanNieuwenhze, S. H. White, J. L. Witztum and E. A. Dennis, *J. Lipid Res.*, 2005, **46**, 839–862.

53 E. Fahy, M. Sud, D. Cotter and S. Subramaniam, *Nucleic Acids Res.*, 2007, **35**, W606–W612.

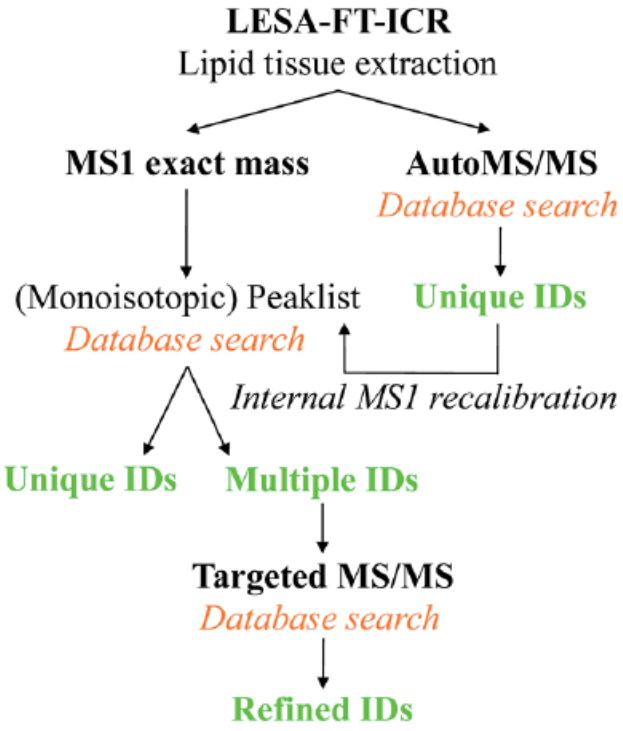

Figure 1: LESA-FT-ICR workflow developed in this study.

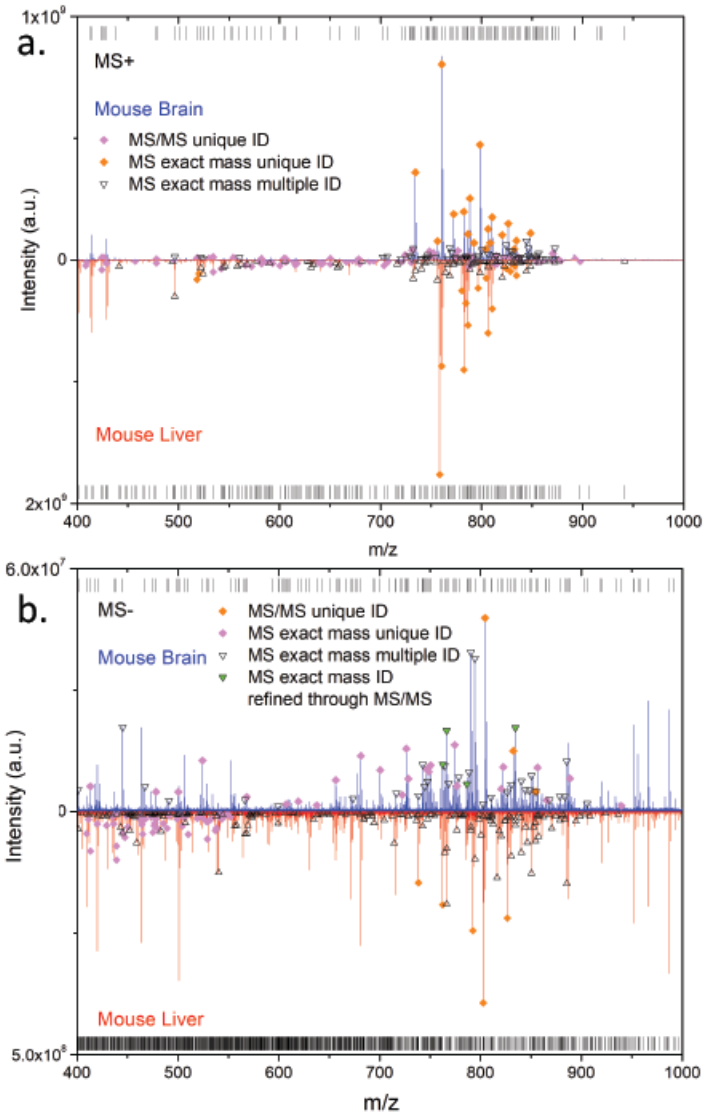

Figure 2: Positive (a.) and negative (b.) ionization mode LESA-FT-ICR MS spectra of mouse brain (top, blue) and of mouse liver (bottom, red). The vertical lines on top of each spectrum represent the monoisotopic m/z peaks extracted for identification. The orange markers denote MS/MS identified peaks. The m/z peaks with unique and multiple lipid identifications are highlighted with pink and black markers. As proof-of-concept, the negative mode analysis of MB was subjected to targeted MS/MS experiments using MS1 accurate mass assignments (highlighted with green triangular markers).

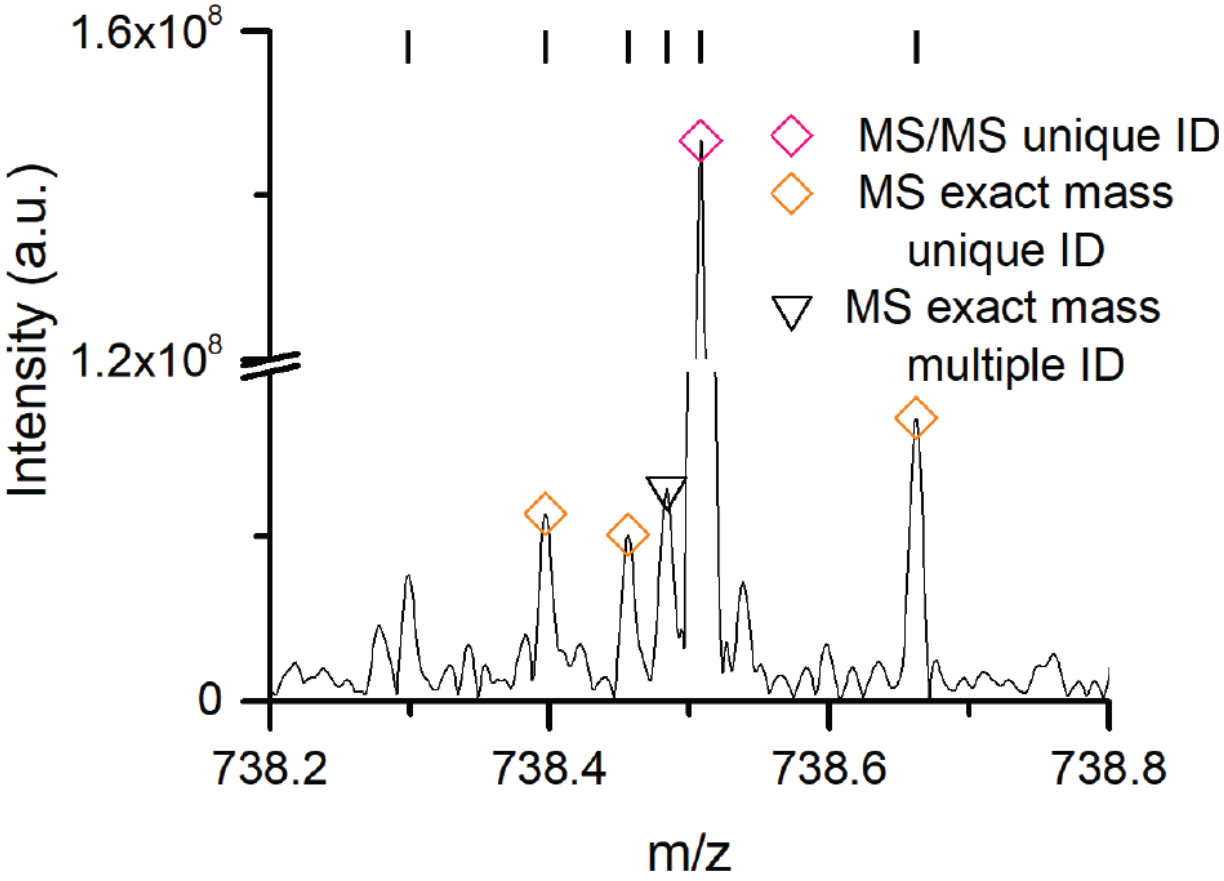

Figure 3: Extract from the mouse liver mass spectrum in negative mode from m/z 738.2 to 738.8. The black vertical lines represent the monoisotopic m/z peaks extracted for identification. The orange markers denote MS/MS identified peaks. The m/z peaks with unique and multiple lipid identifications are highlighted with pink and black markers.

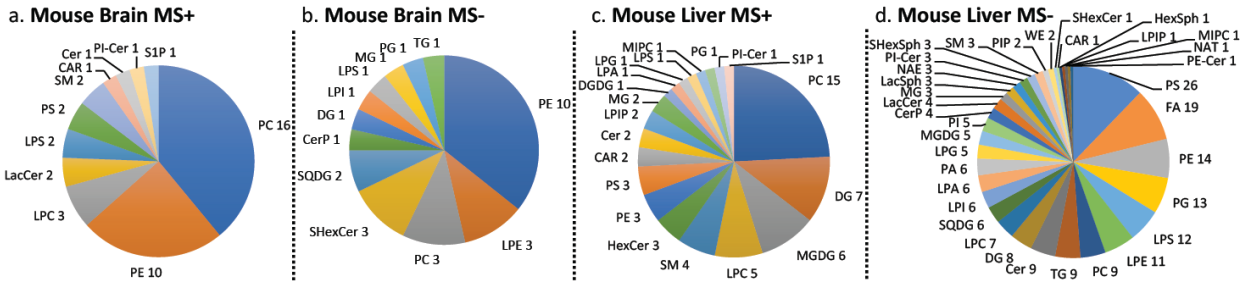

Figure 4: Representations of the identified lipid classes in MB and ML (from both MS/MS and MS1), weighted by the number of unique and distinct lipid identifications for each class. a. and c. represent positive ionization for MB and ML, respectively, and b. and d. represent negative ionization for both samples.

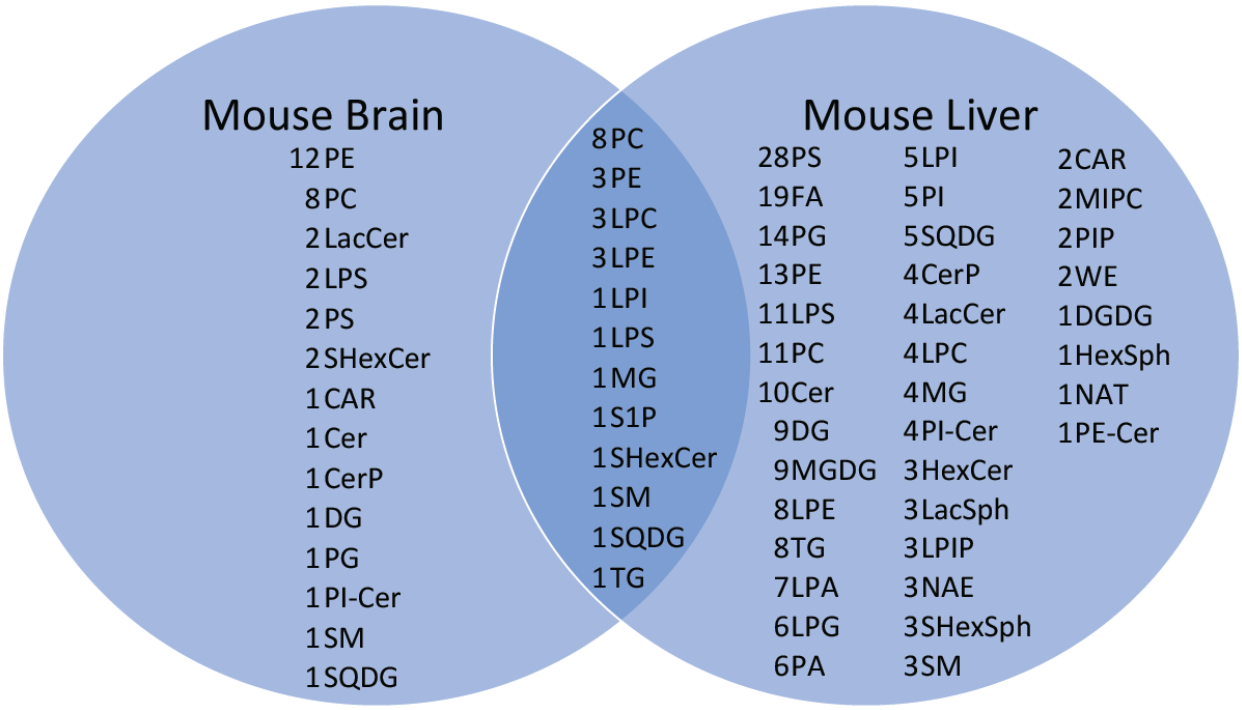

Figure 5: Diagram of the lipid compositions (lipid classes) of healthy mouse brain and mouse liver samples identified from LESA-FT-ICR-MS (MS/MS and MS1) measurements, including both positive and negative ionization mode. The circle overlap represents the number of distinct lipids from the different lipid classes which were found in both tissues.

Mouse Brain MS+

ID	Precursor	Species	Chemical	Main	Short	Theo.	ppm	Identified fragments
1	426.3568	$[M+H]^+$	C25H48NO4	CAR	CAR(18:1)	426.36	2.35	MS1
2	604.5059	$[M+K]^+$	C36H71NO3K	Cer	Cer(d36:1)	604.51	1.06	MS1
3	836.6082	$[M+H]^+$	C44H86NO13	LacCer	LacCer(d32:0)	836.61	1.41	MS1
4	854.5578	$[M+Na]^+$	C44H81NO13Na	LacCer	LacCer(d32:2)	854.56	2.57	MS1
5	478.3282	$[M+H-H2O]^+$	C24H49NO6P	LPC	LPC(16:0)	478.33	2.17	MS1*
5	518.3208	$[M+Na]^+$	C24H50NO7PNa	LPC	LPC(16:0)	518.32	1.77	MS1*
5	534.2947	$[M+K]^+$	C24H50NO7PK	LPC	LPC(16:0)	534.3	1.63	MS1*
6	582.2949	$[M+K]^+$	C28H50NO7PK	LPC	LPC(20:4)	582.3	1.27	MS1
7	606.2951	$[M+K]^+$	C30H50NO7PK	LPC	LPC(22:6)	606.3	0.82	MS1
8	530.2868	$[M+H-H2O]^+$	C26H45NO8P	LPS	LPS(20:3)	530.29	1.62	MS1
9	554.2869	$[M+H-H2O]^+$	C28H45NO8P	LPS	LPS(22:5)	554.29	1.50	MS1
10	734.5693	$[M+H]^+$	C40H81NO8P	PC	PC(32:0)	734.5694	0.11	HG (184.0725)
11	760.5851	$[M+H]^+$	C42H83NO8P	PC	PC(34:1)	760.5851	0.00	HG (184.0725)
12	756.5514	$[M+H]^+$	C42H79NO8P	PC	PC(34:3)	756.5538	3.16	HG (184.0724)
13	788.6166	$[M+H]^+$	C44H87NO8P	PC	PC(36:1)	788.6164	-0.25	HG (184.0725)
14	786.6009	$[M+H]^+$	C44H85NO8P	PC	PC(36:2)	786.6007	-0.26	HG (184.0725)
15	782.5666	$[M+H]^+$	C44H81NO8P	PC	PC(36:4)	782.5694	3.64	HG (184.0725)
15	820.5258	$[M+K]^+$	C44H80NO8PK	PC	PC(36:4)	820.5253	-0.58	M-C5H13NO3P-H2O (637.4541)
16	810.6014	$[M+H]^+$	C46H85NO8P	PC	PC(38:4)	810.6007	-0.87	HG (184.0725)
16	848.5572	$[M+K]^+$	C46H84NO8PK	PC	PC(38:4)	848.5566	-0.74	M-C5H13NO3P-H2O (665.4851)
17	808.5858	$[M+H]^+$	C46H83NO8P	PC	PC(38:5)	808.5851	-0.85	HG (184.0725)
18	806.5698	$[M+H]^+$	C46H81NO8P	PC	PC(38:6)	806.5694	-0.46	HG (184.0725)
19	804.5517	$[M+H]^+$	C46H79NO8P	PC	PC(38:7)	804.5538	2.65	HG (184.0725)
20	834.6013	$[M+H]^+$	C48H85NO8P	PC	PC(40:6)	834.6007	-0.67	HG (184.0725)
21	832.5833	$[M+H]^+$	C48H83NO8P	PC	PC(40:7)	832.5851	2.20	HG (184.0725)
21	870.5417	$[M+K]^+$	C48H82NO8PK	PC	PC(40:7)	870.54	-0.83	MS1*
22	892.5261	$[M+K]^+$	C50H80NO8PK	PC	PC(42:10)	892.53	-0.85	MS1
23	772.5254	$[M+H]^+$	C45H75NO7P	PC	PC(O-37:9)	772.5276	2.75	HG (184.0725)
24	798.5412	$[M+H]^+$	C47H77NO7P	PC	PC(O-39:10)	798.5432	2.54	HG (184.0725)
25	826.5728	$[M+H]^+$	C49H81NO7P	PC	PC(O-41:10)	826.5745	2.10	HG (184.0728)
26	650.4388	$[M+H]^+$	C33H65NO9P	PE	PE(28:1(OH))	650.44	0.52	MS1*
27	678.4703	$[M+H]^+$	C35H69NO9P	PE	PE(30:1(OH))	678.47	0.13	MS1*
28	792.5540	$[M+H]^+$	C45H79NO8P	PE	PE(40:6)	792.5538	-0.29	M-C2H7NO3P-H2O (651.5296)
29	828.4945	$[M+K]^+$	C45H76NO8PK	PE	PE(40:7)	828.49	-0.60	MS1*
30	724.5276	$[M+H]^+$	C41H75NO7P	PE	PE(O-36:5) or PE(P-36:4)	724.5276	0.01	MS1
31	752.5589	$[M+H]^+$	C43H79NO7P	PE	PE(O-38:5) or PE(P-38:4)	752.5589	-0.04	MS1
31	790.5150	$[M+K]^+$	C43H78NO7PK	PE	PE(O-38:5) or PE(P-38:4)	790.5147	-0.38	MS1
32	750.5434	$[M+H]^+$	C43H77NO7P	PE	PE(O-38:6) or PE(P-38:5)	750.5432	-0.28	MS1
33	780.5904	$[M+H]^+$	C45H83NO7P	PE	PE(O-40:5) or PE(P-40:4)	780.5902	-0.31	MS1
34	748.5275	$[M+H]^+$	C43H75NO7P	PE	PE(P-38:6)	748.53	0.11	MS1
34	786.4836	$[M+K]^+$	C43H74NO7PK	PE	PE(P-38:6)	786.48	-0.29	MS1
35	776.5591	$[M+H]^+$	C45H79NO7P	PE	PE(P-40:6)	776.56	-0.22	MS1
35	814.5151	$[M+K]^+$	C45H78NO7PK	PE	PE(P-40:6)	814.51	-0.49	MS1
36	876.5731	$[M+K]^+$	C44H88NO11PK	PI-Cer	PI-Cer(d38:0)	876.57	-0.48	MS1*
37	822.5238	$[M+Na]^+$	C43H78NO10PNa	PS	PS(37:3)	822.53	2.25	MS1
38	774.5234	$[M+Na]^+$	C39H78NO10PNa	PS	PS(O-33:0(OH))	774.53	2.79	MS1
39	424.2813	$[M+H]^+$	C20H43NO6P	S1P	S1P(t20:1)	424.28	2.07	MS1*
40	731.6060	$[M+H]^+$	C41H84N2O6P	SM	SM(d36:1)	731.61	0.14	MS1*
41	753.5882	$[M+Na]^+$	C41H83N2O6PNa	SM	SM(d36:1)	753.59	-0.17	MS1*
42	813.6846	$[M+H]^+$	C47H94N2O6P	PE	SM(d42:2)	813.68	-0.23	MS1*

Mouse Liver MS+

ID	Precursor	Species	Chemical	Main	Short	Theo.	ppm	Identified fragments
1	408.3074	$[M+Na]^+$	C22H43NO4Na	CAR	CAR(15:0)	408.3084	-2.50	MS1
2	428.3724	$[M+H]^+$	C25H50NO4	CAR	CAR(18:0)	428.3734	-2.38	MS1
3	638.6075	$[M+H]^+$	C40H80NO4	Cer	Cer(t40:1)	638.6082	-1.05	MS1*
4	666.6390	$[M+H]^+$	C42H84NO4	Cer	Cer(t42:1)	666.6395	-0.80	MS1
5	589.4795	$[M+Na]^+$	C35H66O5Na	DG	DG(32:1)	589.4802	-1.19	MS1
6	617.5108	$[M+Na]^+$	C37H70O5Na	DG	DG(34:1)	617.5115	-1.07	MS1
7	615.4952	$[M+Na]^+$	C37H68O5Na	DG	DG(34:2)	615.4959	-1.19	MS1
8	613.4795	$[M+Na]^+$	C37H66O5Na	DG	DG(34:3)	613.4802	-1.08	MS1
9	643.5266	$[M+Na]^+$	C39H72O5Na	DG	DG(36:2)	643.5272	-0.95	MS1
10	641.5109	$[M+Na]^+$	C39H70O5Na	DG	DG(36:3)	641.5115	-0.87	MS1
11	639.4952	$[M+Na]^+$	C39H68O5Na	DG	DG(36:4)	639.4959	-1.05	MS1
12	897.5922	$[M+H-H2O]+$	C49H85O14	DGDG	DGDG(34:3)	897.5934	-1.35	MS1
13	572.4513	$[M+H-H2O]^+$	C32H62NO7	HexCer	HexCer(d26:0)	572.4521	-1.48	MS1
14	586.4670	$[M+H-H2O]^+$	C33H64NO7	HexCer	HexCer(d27:0)	586.4677	-1.28	MS1
15	600.4826	$[M+H-H2O]^+$	C34H66NO7	HexCer	HexCer(d28:0)	600.4834	-1.27	MS1
16	409.2340	$[M+H]^+$	C19H38O7P	LPA	LPA(16:1)	409.2350	-2.42	MS1
17	478.3282	$[M+H-H2O]^+$	C24H49NO6P	LPC	LPC(16:0)	478.3292	-2.13	MS1*
17	534.2947	$[M+K]^+$	C24H50NO7PK	LPC	LPC(16:0)	534.2956	-1.65	MS1*
18	520.3388	$[M+H]^+$	C26H51NO7P	LPC	LPC(18:2)	520.3398	-1.80	M-C21H37O6P (104.1068), HG (184.0725), M-H2O (502.3254)
18	542.3208	$[M+Na]^+$	C26H50NO7PNa	LPC	LPC(18:2)	542.3217	-1.64	MS1
19	518.3208	$[M+H]^+$	C26H49NO7P	LPC	LPC(18:3)	518.3241	-6.49	M-C21H35O6P (104.1068), HG (184.0725)
20	582.2948	$[M+K]^+$	C28H50NO7PK	LPC	LPC(20:4)	582.2956	-1.31	MS1
20	566.3209	$[M+Na]^+$	C28H50NO7PNa	LPC	LPC(20:4)	566.3217	-1.39	MS1
21	606.2949	$[M+K]^+$	C30H50NO7PK	LPC	LPC(22:6)	606.2956	-1.09	MS1
22	495.3073	$[M+H-H2O]^+$	C24H48O8P	LPG	LPG(18:0)	495.3081	-1.72	MS1
23	689.2106	$[M+K]^+$	C25H48O15P2K	LPIP	LPIP(16:1)	689.2100	0.93	MS1
24	839.3513	$[M+K]^+$	C36H66O15P2K	LPIP	LPIP(27:3)	839.3509	0.44	MS1
25	580.3601	$[M+H]^+$	C28H55NO9P	LPS	LPS(22:1)	580.3609	-1.33	MS1
26	429.2966	$[M+Na]^+$	C25H42O4Na	MG	MG(22:4)	429.2975	-2.05	MS1
27	457.3279	$[M+Na]^+$	C27H46O4Na	MG	MG(24:4)	457.3288	-1.88	MS1
28	593.3288	$[M+Na]^+$	C30H50O10Na	MGDG	MGDG(21:3)	593.3296	-1.35	MS1
29	665.4232	$[M+Na]^+$	C35H62O10Na	MGDG	MGDG(26:2)	665.4235	-0.48	MS1
30	679.4389	$[M+Na]^+$	C36H64O10Na	MGDG	MGDG(27:2)	679.4392	-0.40	MS1
31	693.4546	$[M+Na]^+$	C37H66O10Na	MGDG	MGDG(28:2)	693.4548	-0.26	MS1
32	707.4703	$[M+Na]^+$	C38H68O10Na	MGDG	MGDG(29:2)	707.4705	-0.30	MS1
33	721.4859	$[M+Na]^+$	C39H70O10Na	MGDG	MGDG(30:2)	721.4861	-0.22	MS1
34	878.5396	$[M+H-H2O]^+$	C44H81NO14P	MIPC	MIPC(m32:2)	878.5389	0.75	MS1
35	730.5380	$[M+H]^+$	C40H77NO8P	PC	PC(32:2)	730.5381	-0.14	MS1*
36	760.5851	$[M+H]^+$	C42H83NO8P	PC	PC(34:1)	760.5851	0.02	HG (184.0725), M-FA 18:1 (496.3364)
37	758.5694	$[M+H]^+$	C42H81NO8P	PC	PC(34:2)	758.5694	0.00	HG (184.0725)
38	786.6009	$[M+H]^+$	C44H85NO8P	PC	PC(36:2)	786.6007	0.18	HG (184.0725)
39	784.5853	$[M+H]^+$	C44H83NO8P	PC	PC(36:3)	784.5851	0.21	HG (184.0725)
40	782.5697	$[M+H]^+$	C44H81NO8P	PC	PC(36:4)	782.5694	0.33	HG (184.0725)
41	780.5513	$[M+H]^+$	C44H79NO8P	PC	PC(36:5)	780.5538	-3.18	HG (184.0725)
42	810.6011	$[M+H]^+$	C46H85NO8P	PC	PC(38:4)	810.6007	0.48	HG (184.0725), M-C5H13NO3P-H2O (627.5343)
43	806.5698	$[M+H]^+$	C46H81NO8P	PC	PC(38:6)	806.5694	0.49	HG (184.0725)
44	804.5515	$[M+H]^+$	C46H79NO8P	PC	PC(38:7)	804.5538	-2.84	HG (184.0725)
45	834.6013	$[M+H]^+$	C48H85NO8P	PC	PC(40:6)	834.6007	0.66	HG (184.0725), M-C5H13NO3P-H2O (651.5293)
46	832.5857	$[M+H]^+$	C48H83NO8P	PC	PC(40:7)	832.5851	0.72	HG (184.0725)
46	870.5418	$[M+K]^+$	C48H82NO8PK	PC	PC(40:7)	870.5410	0.88	MS1*
47	828.5518	$[M+H]^+$	C48H79NO8P	PC	PC(40:9)	828.5538	-2.37	HG (184.0724), M-C5H13NO3P-H2O (546.4805)
48	796.5255	$[M+H]^+$	C47H75NO7P	PC	PC(O-39:11)	796.5276	-2.60	HG (184.0725)
49	824.5571	$[M+H]^+$	C49H79NO7P	PC	PC(O-41:11)	824.5589	-2.20	HG (184.0725)
50	650.4386	$[M+H]^+$	C33H65NO9P	PE	PE(28:1(OH))	650.4391	-0.75	MS1*
50	672.4207	$[M+Na]^+$	C33H64NO9PNa	PE	PE(28:1(OH))	672.4211	-0.64	MS1*
51	676.4544	$[M+H]^+$	C35H67NO9P	PE	PE(30:2(OH))	676.4548	-0.55	MS1*
52	790.5391	$[M+H]^+$	C45H77NO8P	PE	PE(40:7)	790.5381	1.21	MS1*
53	789.4676	$[M+Na]^+$	C42H71O10PNa	PG	PG(36:6)	789.4677	-0.13	MS1*
54	860.5057	$[M+K]^+$	C42H80NO12PK	PI-Cer	PI-Cer(t36:2)	860.5050	0.84	MS1*
55	858.5861	$[M+H]^+$	C46H85NO11P	PS	PS(40:3(OH))	858.5855	0.72	MS1
56	854.5549	$[M+H]^+$	C46H81NO11P	PS	PS(40:5(OH))	854.5542	0.77	MS1
57	718.4624	$[M+Na]^+$	C35H70NO10PNa	PS	PS(O-29:0(OH))	718.4630	-0.82	MS1
58	424.2813	$[M+H]^+$	C20H43NO6P	S1P	S1P(t20:1)	424.2822	-2.05	MS1*
59	703.5745	$[M+H]^+$	C39H80N2O6P	SM	SM(d34:1)	703.5748	-0.38	MS1*
60	787.6690	$[M+H]^+$	C45H92N2O6P	SM	SM(d40:1)	787.6687	0.32	MS1*
61	815.7005	$[M+H]^+$	C47H96N2O6P	SM	SM(d42:1)	815.7000	0.56	MS1*
62	813.6848	$[M+H]^+$	C47H94N2O6P	SM	SM(d42:2)	813.6844	0.50	MS1*

Table 1: Summary of the positive ionization mode LESA-FT-ICR-MS (MS1 and MS/MS) of a MB (left) and ML (right) sample. The molecular ion species, chemical composition, lipid class, theoretical mass, mass error, and identifiers are provided. HG denotes the head group and FA denotes fatty acids. MS1* designates lipid identifications where odd-chained lipids were discarded as biologically unlikely.

Mouse Brain MS- with multiple MS1 identifications								
Precursor *m/z*	species	Chemical Composition	Main Class	Short Name	Theo. *m/z*	ppm	Identified fragments from MS/MS	MS/MS refined identification
762.5079	$[M-H]^-$	C43H73NO8P	PE	PE(38:6)	762.5079	0.05	FA 16:0(+COO) (255.2306), FA 22:6(-CO) (283.2423), FA 22:6(+COO) (327.2305), M-FA 22:6(-H) (452.2765)	PE(22:6_16:0)
	$[M-H]^-$	C43H73NO8P	PE	PE(P-38:6(OH))	762.5079	0.05		
766.5393	$[M-H]^-$	C43H77NO8P	PE	PE(38:4)	766.5392	0.14	FA 18:0(+COO) (283.2615), FA 20:4(+COO) (303.2312), M-FA 20:4(+COO) (480.3029)	PE(20:4_18:0)
	$[M-H]^-$	C43H77NO8P	PE	PE(O-38:5(OH)) or PE(P-38:4(OH))	766.5392	0.14		
786.5276	$[M+HCOO]^-$	C42H77NO10P	PC	PC(33:3)	786.5291	-1.91		
	$[M+HCOO]^-$	C42H77NO10P	PE	PE(36:3)	786.5291	-1.91		
	$[M+HCOO]^-$	C42H77NO10P	PE	PE(O-36:4(OH)) or PE(P-36:3(OH))	786.5291	-1.91		
	$[M-H]^-$	C42H77NO10P	PS	PS(36:2)	786.5291	-1.91	FA 18:1(+COO) (281.2468), M-FA 18:1(+HO)-C3H5NO2 (417.2372), M-C3H5NO2 (699.4904)	PS(18:1_18:1)
	$[M-H]^-$	C42H77NO10P	PS	PS(O-36:3(OH)) or PS(P-36:2(OH))	786.5291	-1.91	FA 18:1(+COO) (281.2468), M-FA 18:1(+HO)-C3H5NO2 (417.2372), M-C3H5NO2 (699.4904)	PS(O-18:1_18:1(OH)) or PS(P-18:0_18:1(OH))
834.529	$[M+HCOO]^-$	C46H77NO10P	PC	PC(37:7)	834.5291	-0.07		
	$[M+HCOO]^-$	C46H77NO10P	PE	PE(40:7)	834.5291	-0.07		
	$[M-H]^-$	C46H77NO10P	PS	PS(40:6)	834.5291	-0.07	FA 22:6(-CO) or FA 18:0(+O) (283.2643), FA 22:6(+O) (327.2323), FA 22:6(+OH) (419.2576), M-FA 20:1(+HO)-C3H5NO2 or FA 22:6(-H)-C3H5NO2 (437.2675), M-FA 18:0(+HO)-C3H5NO2 or FA 20:5-C3H5NO2 (463.2265), M-C3H5NO2 (747.4984)	PS(22:6_18:0) or PS(20:1_20:5)
	$[M-H]^-$	C46H77NO10P	PS	PS(P-40:6(OH))	834.5291	-0.07	FA 18:1(+O) (281.2489), FA 22:6(-CO) or FA 18:0(+O) (283.2643), FA 20:4(+O) or FA 23:3(-CO) (303.2339), FA 22:6(+O) or FA 25:5(-CO) (327.2323), FA 23:4(-H)-C3H5NO2 or FA 22:6(+OH) (419.2576), M-FA 20:1(+HO)-C3H5NO2 or FA 22:6(-H)-C3H5NO2 (437.2675), M-FA 18:0(+HO)-C3H5NO2 or FA 20:5-C3H5NO2 (463.2265), M-C3H5NO2 (747.4984)	PS(P-23:4_17:2(OH)) or PS(P-23:3_17:3(OH)) or PS(P-22:6_18:0(OH)) or PS(P-20:4_20:2(OH)) or PS(P-20:1_20:5(OH)) or PS(P-18:1_22:5(OH))

Table 2: Negative ion mode targeted MS/MS after preliminary MS1 accurate mass database search from the MB. The different lipid identification possibilities are shown, with the MS/MS fragment ion interpretations which refine the m/z identification.